STATE OF THE CLIMATE IN 2016

Special Supplement to the
Bulletin of the American Meteorological Society
Vol. 98, No. 8, August 2017

basin. Through June and July, these anomalies intensified and propagated east and south, as the current is deflected off the equator by the presence of the Malaysian coast. The anomalies weakened slightly in August, then persisted at approximately the same strength (30–35 cm s^{-1} eastward in the region 6°–8°S, 80°–100°E) through the end of 2016.

The Agulhas Current transport is a key indicator of Indian–Atlantic Ocean interbasin water exchanges. The annual mean transport of the Agulhas Current decreased over the period 2013–15, from 56 Sv (1 Sv ≡ 10^6 m^3 s^{-1}) in 2013 to 50 Sv in 2015 (www.aoml.noaa.gov/phod/altimetry/cvar). In 2016, the Agulhas Current had an annual average transport of 54 Sv, exceeding the long-term mean of 50 Sv. These changes are larger than the ~3 Sv standard deviation of the individual yearly estimates.

3) Atlantic Ocean

Annual mean anomalies in the Atlantic Ocean (Fig. 3.18a) indicate an 8–10 cm s^{-1} strengthening of the eastward NECC and comparable weakening of the westward northern South Equatorial Current (nSEC) at 2°–5°N, 15°–40°W. Elsewhere, conditions were near climatology. Because anomalies were weaker in 2015, the 2016 minus 2015 map (Fig. 3.18b) closely resembles the 2016 map. Looking at the month-to-month development of anomalies, large-scale conditions were close to climatology until May, when eastward anomalies began developing across the equatorial band, indicating a slowing of the westward nSEC. By June, these anomalies exceeded 20 cm s^{-1} at 1°–3°N, 0°–30°W. They then weakened through July and August, when eastward anomalies began developing to the north, in the latitude band of the NECC. These anomalies, which dominated the annual average, intensified through September–November in the western NECC and were still present at the end of the year. Averaged over the last four months of the year, eastward anomalies peaked at 30 cm s^{-1} at 4°N, 30°–45°W. Weaker westward anomalies centered at 6°N in the same longitude band indicate that the NECC was not only stronger, but also shifted somewhat south of its climatological position.

The mean position of the Gulf Stream extension shifted north by approximately 0.5° latitude in 2016 relative to climatological values (see Sidebar 3.1 for related impacts), while the Loop Current did not extend as fully into the Gulf of Mexico on average in 2016 as it had in the previous two years.

In the southwest Atlantic Ocean, the Brazil Current carries waters from subtropical to subpolar regions mainly in the form of large anticyclonic rings (Lentini et al. 2006). The separation of the Brazil Current front from the continental shelf break continued to exhibit annual periodicity (www.aoml.noaa.gov/phod/altimetry/cvar), which is mainly driven by wind stress curl variations and the transport of this current. During 1993–2005, the annual mean separation of the front shifted southward in response to a long-term warming in South Atlantic temperatures (cf. Lumpkin and Garzoli 2011; Goni et al. 2011). Since 2005, the location of the front has not exhibited interannual trends. The year 2016 was an anomalous one in which the front was persistently shifted north of its long-term mean position—something not seen since 1994. It remains to be seen if this represents a transient or more sustained reversal of the long-term shift of the confluence to the south.

h. Meridional overturning and oceanic heat transport circulation observations in the North Atlantic Ocean—M. O. Baringer, D. A. Smeed, J. Willis, M. Lankhorst, W. R. Hobbs, S. Dong, G. McCarthy, D. Rayner, W. E. Johns, G. Goni, and U. Send

This section describes the AMOC and the Atlantic meridional heat transport (AMHT), determined by the large-scale ocean circulation wherein northward moving upper layer waters are transformed into deep waters that return southward, redistributing heat, fresh water, carbon, and nutrients. Large variations in meridional heat transport are associated with strong MOC anomalies (e.g., correlations of 0.94, Johns et al. 2011) and northwesterly wind anomalies while monthly variability is more closely linked to the spatial structure associated with the North Atlantic oscillation (NAO; e.g., Moat et al. 2016). Observed cold North Atlantic sea surface temperatures were consistent with the decadal decrease in MOC transport at 26°N (e.g., Baringer et al. 2016). These large-scale ocean anomalies can subsequently impact European weather (e.g., Duchez et al. 2016). Many climate, weather, and ecosystem changes covary with changes in the AMOC (e.g., Srokosz and Bryden 2015; Carton et al. 2014; Srokosz et al. 2012).

The AMOC is computed as the maximum of the vertical accumulation of the horizontally integrated velocity across a zonal-vertical section (i.e., the maximum transport that occurs in either the upper or lower layer before the circulation starts to change direction again). The AMHT involves the covariability of temperature and velocity and is only meaningful as a flux (and hence, independent of the absolute temperature scale used) when the total mass transport can be accounted for (i.e., sums to zero). Observing systems can measure both temperature and velocity, usually with tradeoffs in system design

that favor the computation of one quantity over the other. Here we describe the AMOC from observing systems at 41°N, 26°N, and 16°N and AMHT at 41°N, 26°N, and 35°S.

The longest time series of ocean transport to serve as an index of the AMOC's strength in the North Atlantic (e.g., Frajka-Williams 2015; Duchez et al. 2014) is from the Florida Current (FC, as the Gulf Stream is called at 26°N), measured since 1982 (Fig. 3.21). FC and AMOC transport variations at all time scales also are inversely linked to sea level variations along the U.S. East Coast (e.g., McCarthy et al. 2015). The median 1982–2016 transport of the FC is 31.9 (±0.25) Sv, with the uncertainty being one standard error of the mean assuming a 20-day integral time scale. There is a small downward trend in the record of −0.30 (±0.24) Sv decade^{-1}, this time with 95% significance levels. The 2016 median FC transport was 31.8 (±1.9) Sv, not statistically significantly below the long-term average. Daily FC transports compared to those of all previous years (Fig. 3.21) indicate that 2016, like previous years, included several unusual transport anomalies (extremes defined as outside the 95% confidence limits for daily values). During 2016 there were two high transport events during 31 July–3 August and 10–11 September, with transport in excess of 38.8 Sv. Low transport anomalies occurred during 15–21 April, 10–23 October, and 13–15 November 2016. The lowest daily 2016 FC transport was 19.8 (±1.7) Sv on 18 April, with transports < 23 Sv for five days around this date. Of note is the coincidence of the low transport events in October and November with king tide events in South Florida, which caused widespread street flooding, and the 14 November 2016 "supermoon" (see www.nasa.gov/feature/goddard/2016/novembers-spectacular-supermoon). The difference between the observed sea level at the Lake Worth tide gauge station was larger than the predicted tidal sea level during these events (Fig. 3.21) and inversely correlated with the FC transport at well over the 99% significance level (correlation coefficient −0.62, 37% of variance explained).

In the North Atlantic, the latitudes with currently available AMOC estimates include 41°N, where a combination of profiling Argo floats (that measure ocean temperature and salinity for the upper 2000 m on broad spatial scales, as well as velocity at 1000 m) and altimetry-derived surface velocity (Willis 2010) are used to estimate the AMOC (Fig. 3.22) and AMHT (Fig. 3.23). This time series has been updated since last year's report (Baringer et al. 2016), extending from January 2002 to April 2016. At 26°N, the AMOC (Fig. 3.22) and AMHT (Fig. 3.23) are measured with full-water column moorings that span the full basin and include direct transport measurements in the boundary currents as part of the large RAPID-MOC/MOCHA/WBTS 26°N mooring array (Smeed et al. 2015). The data from this array are collected every 18 months; hence the MOC data shown here extend from April 2004 to October 2015 (MHT data available to April 2014). At 16°N, a mooring array of inverted echo sounders, current meters, and dynamic height moorings (Send et al. 2011) measures the flow below 1000 m (the southward flowing part of the AMOC "conveyor belt") that sends North Atlantic Deep Water toward the equator; hence, the AMOC estimate at this latitude (Fig. 3.22) is a negative number (southward deep flow) to distinguish these observations from the full water column systems. Since this array only measures the deep circulation, an estimate of the AMHT is

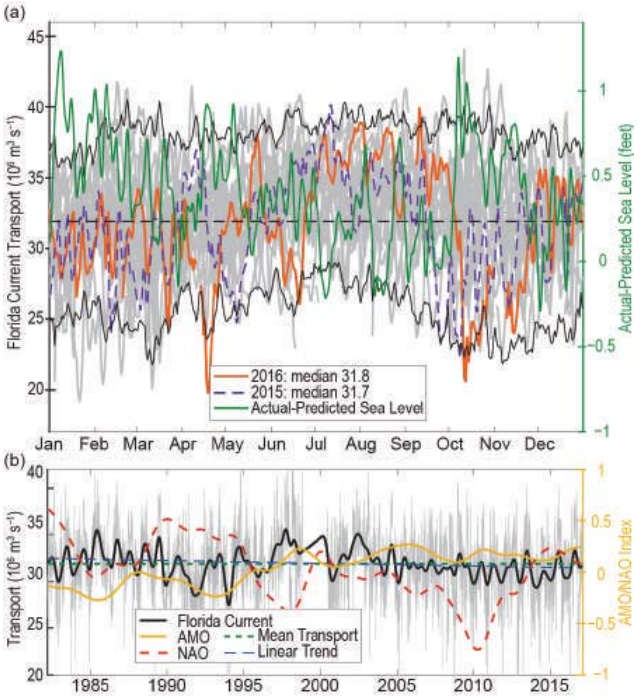

Fig. 3.21. (a) Daily estimates of Florida Current transport (10^6 m^3 s^{-1}) during 2016 (orange solid line), 2015 (dashed purple line), and 1982–2016 (light gray lines) with 95% confidence interval of daily transport values computed from all years (black solid line), the long-term mean (dashed black line), and actual observed sea level at the Lake Worth Pier tide gauge station minus predictions (green line) based on NOAA harmonic tide constituents (https://tidesandcurrents.noaa.gov/stationhome.html?id=8722670). (b) Daily estimates of Florida Current transport (10^6 m^3 s^{-1}) for the full record (light gray), smoothed using a 12-month second-order Butterworth filter (heavy black line), mean transport for the full record (dashed green line), and linear trend for 1982–2016 (dashed blue line). Two-year low-passed AMO (yellow line) and NAO (red dashed line) indices are also shown.

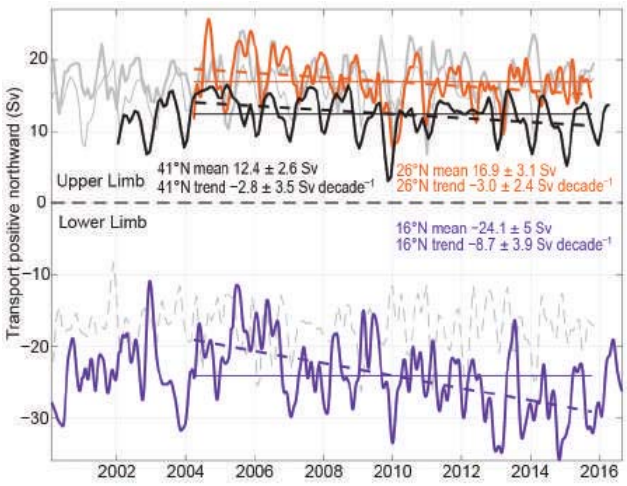

Fig. 3.22. Estimates of 2000–16 AMOC (Sv) from the Argo/Altimetry estimate at 41°N (black; Willis 2010), the RAPID-MOC/MOCHA/WBTS 26°N array (red; McCarthy et al. 2015), and the German/NOAA MOVE array at 16°N (blue; Send et al. 2011); a 3-month second-order Butterworth low-pass filter is also applied. Horizontal lines are mean transports during similar time periods as listed in the corresponding text. Dashed lines are trends for each series. For MOVE data, the net zonal and vertical integral of the deep circulation represents the lower limb of the AMOC (with a negative sign indicating southward flow), and hence a stronger negative (southward) flow represents an increase in the AMOC amplitude. Light gray lines show EC-derived transports (Menemenlis et al. 2008): (top) thin gray is the 41°N transport, thick gray is the 26°N transport, (bottom) shows the negative meridional overturning circulation in the model for ease of comparison with the 16°N data.

impossible at 16°N because of the missed large signals and high correlations in the surface waters. These data have been updated since last year's report and now extend from February 2000 to September 2016. At 35°S in the South Atlantic, the AMHT is estimated using a combination of high-density (closely spaced) expendable bathythermograph (XBT) and broader-scale Argo profiling float data (Dong et al. 2014). While the AMOC has also been estimated at 35°S, those estimates (not shown) are rough because the XBTs only extend to 750 m. These data are collected and analyzed in near-real time, with values spanning July 2002 to August 2016.

In the far North Atlantic the MOC time series continue the relatively low trend in MOC transport: the trend of the MOC at 26°N is –3.0 (±2.4) Sv decade^{-1} (Fig. 3.22) and the MHT trend is –0.23 (±0.19) PW decade^{-1} (1 PW = 10^{15} W; Fig. 3.23). At 41°N these trends are –1.2 (±3.0) Sv decade^{-1} and –0.09 (±0.21) PW decade^{-1}. These values are for the full length of each time series, while Fig. 3.22 lists the trends for the overlapping time periods of each time series (denoted by the dashed line in each panel). These trends are not statistically significantly less than those in last year's report (–4.1 (±3.2) Sv decade^{-1} and –0.23 (±0.19) PW decade^{-1} at 26°N and –1.3 (±4.9) Sv decade^{-1} and –0.15 (±0.27) PW decade^{-1} at 41°N), despite slightly larger MOC and MHT transports reported this year (e.g., at 26°N, the mean MOC increased from 16.0 Sv in 2014 to 16.3 Sv in 2015, and at 41°N, the mean MOC increased from 10.7 Sv in 2015 to 12.5 Sv in 2016). As more data become available, the 26°N data show flow compensation between the FC and upper flows in the center of the ocean, resulting in recirculation that is not associated with a change in the MOC (Frajka-Williams et al. 2016).

Farther south, the MOC and MHT trends are positive but decreasing in the past three years as the annual means at 16°N reduced in magnitude from –29.2 Sv in 2014, to –27.8 Sv in 2015, and then to –23.8 in 2016. The trend of the AMOC from February 2000 to September 2016 at 16°N is +3.4 (±2.4) Sv decade^{-1}

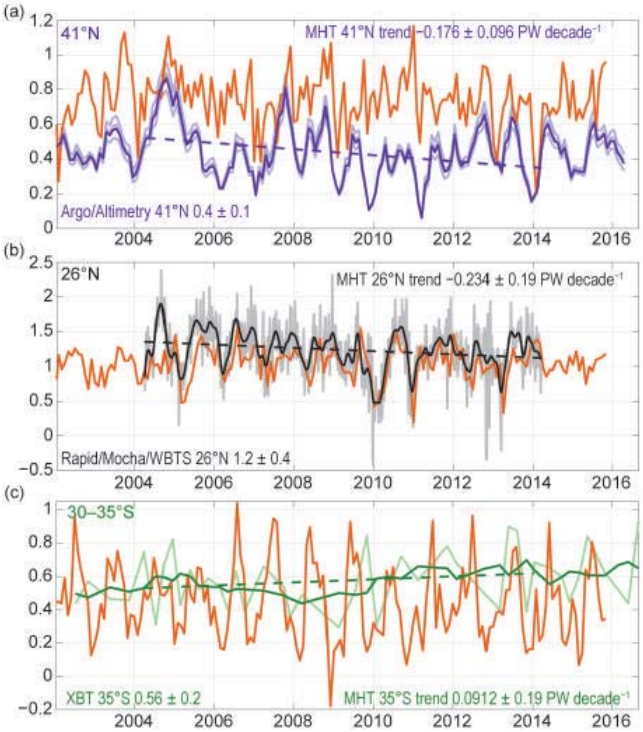

Fig. 3.23. AMHT; (PW) at (a) 41°N (from profiling floats following Hobbs and Willis 2012; blue lines), with uncertainties (light blue lines) and the trend (dashed blue line); at (b) 26°N (from mooring/hydrography data) 12-hourly values (gray line), filtered with a 3-month low-pass filter (black line), and the trend (black dashed line); and at (c) 30°–35°S (from XBTs) quarterly values (light green), filtered with yearly boxcar (dark green line), and the trend (dashed green line). Heat transports simulated by EC (orange lines; Menemenlis et al. 2008) are shown at all latitudes.

(statistically indistinguishable from the trend of +3.6 (±2.5) Sv decade^{-1} reported last year). Similarly, the 35°S AMHT transport estimate has remained fairly constant for the last three years (mean northward values of 0.60 PW in 2014, 0.69 PW in 2015, and 0.63 PW in 2016). These estimates imply a virtually steady AMOC as well (the AMOC and AMHT being highly correlated). The AMHT trend at 35°S from July 2002 to August 2016 is +0.09 (±0.10) PW decade^{-1} (again statistically indistinguishable from the trend of +0.11 (±0.10) PW decade^{-1} reported last year). Variability at all latitudes in the Atlantic is not well correlated, and therefore, data from more than one latitude are needed to describe the state of the ocean. Interannual and higher frequencies dominate the variability in the MOC and MHT time series, and therefore long records will be needed to determine decadal and longer variability.

i. Global ocean phytoplankton—B. A. Franz, M. J. Behrenfeld, D. A. Siegel, and S. R. Signorini

Marine phytoplankton contribute roughly half the net primary production (NPP) on Earth, fixing atmospheric CO_2 into food that fuels global ocean ecosystems and drives biogeochemical cycles (e.g., Field et al. 1998; Falkowski et al. 1998). Satellite ocean color sensors, such as SeaWiFS (McClain 2009), MODIS (Esaias et al. 1998), and VIIRS (Oudrari et al. 2015), provide observations of sufficient frequency and geographic coverage to globally monitor changes in the near-surface concentrations of the phytoplankton pigment chlorophyll-a (Chl*a*; mg m^{-3}) that serve as a proxy for phytoplankton abundance. Here, global Chl*a* distributions for 2016 are evaluated within the context of the 19-year continuous record provided through the combined observations of SeaWiFS (1997–2010), MODIS on *Aqua* (MODISA, 2002–present), and VIIRS on Suomi-NPP (2011–present). All Chl*a* data used in this analysis correspond to version R2014.0 (https://oceancolor.gsfc.nasa.gov/reprocessing), which utilized common algorithms and calibration methods to maximize consistency in the multi-mission satellite record.

The spatial distribution of VIIRS annual mean Chl*a* for 2016 (Fig. 3.24) is consistent with the well-established, physically driven distribution of nutrients (Siegel et al. 2013) and surface mixed-layer light conditions (Behrenfeld et al. 2016). To assess changes in this distribution during 2016, mean values for VIIRS Chl*a* in each month of the year were subtracted from monthly climatological means for MODISA (2003–11). These monthly fields were then averaged to produce the global chlorophyll anomaly map for 2016

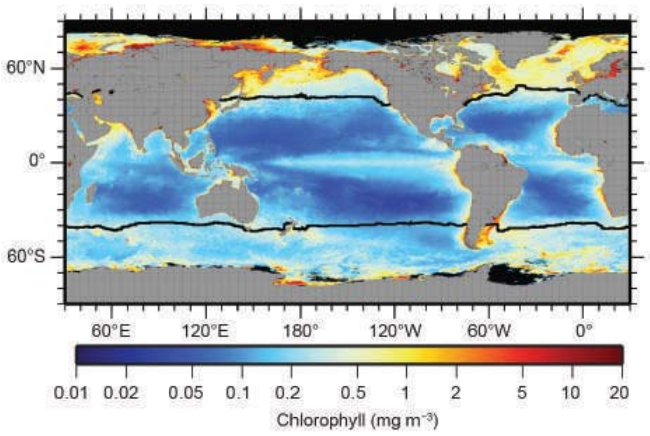

Fig. 3.24. Annual mean Chl*a* distribution (mg m^{-3}) derived from VIIRS for year 2016. Also shown is the location of the mean 15°C SST isotherm (black lines) delineating the boundary of the PSO. Chl*a* data are from NASA Reprocessing version 2014.0. Data are averaged into geo-referenced equal area bins of approximately 4.6 × 4.6 km^2 and mapped to an equirectangular projection centered at 150°W.

(Fig. 3.25a). Identical calculations were performed on MODISA sea surface temperature (SST; °C) data to produce an equivalent SST annual mean anomaly (Fig. 3.25b). The relationship between resultant annual anomalies in Chl*a* and SST are shown in Fig. 3.25c.

The dominant driver of phytoplankton Chl*a* change during 2016 was a climatic shift from El Niño to La Niña conditions. Accordingly, Chl*a* concentrations along the equatorial Pacific were elevated by 10%–20% over the climatological mean (red band in eastern equatorial Pacific in Fig. 3.25a). To the north and south of this band, Chl*a* concentrations were diminished relative to climatological values and inversely related with SST anomalies (dark blue areas above and below the equator in Fig. 3.25c). Within the boundaries of the permanently stratified ocean (PSO), delineated by the black lines in Figs. 3.24 and 3.25 at approximately 40°N and 40°S and defined as the region where annual average surface temperatures are >15°C (Behrenfeld et al. 2006), an inverse relationship was generally observed between Chl*a* and SST anomalies in the South Pacific (dark blue and dark red colors in Fig. 3.25c). By contrast, Pacific regions of the PSO north of the equator exhibited roughly an equal mix of positive and inverse relationships between Chl*a* and SST anomalies. Similarly, a mixture of Chl*a*–SST relationships was observed throughout the Atlantic and Indian sectors of the PSO. These findings for 2016 contrast with some previous findings (e.g., Behrenfeld et al. 2006, 2008, 2009; O'Malley et al. 2010; Siegel et al. 2012; Franz et al. 2013) and are further discussed below. In regions outside the PSO,